International Communications in Heat and Mass Transfer 154 (2024) 107418

Contents lists available at ScienceDirect

International Communications in Heat and Mass Transfer

journal homepage: www.elsevier.com/locate/ichmt

Numerical analysis study on determination of unfrozen water saturation curve for sandy soil

Seok Yoon [a], Gyu-Hyun Go [b,*]

[a] Disposal Safety Evaluation Research Division, KAERI, Daejeon 34057, South Korea
[b] Department of Civil Engineering, Kumoh National Institute of Technology, Gumi, Gyeongbuk 39177, South Korea

ARTICLE INFO

Keywords:
Frozen sandy soil
Unfrozen-water saturation curve
Numerical analysis
Needle probe test
Analytical solution

ABSTRACT

The presence of unfrozen water in frozen soils considerably affects the thermal, hydraulic, and mechanical behaviors of the ground. A thorough examination and accurate estimation of the unfrozen-water saturation curve of target soil materials are required to reliably predict the behavior of frozen soils. This study presents a methodology for accurately determining the curve-fitting coefficients included in an empirical model equation. This study differentiates itself from existing research by presenting a method for easily determining the fitting curve coefficient of empirical unfrozen water saturation model through simple freezing experiment data (time-temperature data) and iterative calculation of numerical analysis. An appropriate unfrozen-water saturation curve of sandy soil specimens was obtained by conducting iterative numerical analyses based on indoor experimental data. The reliability of the determined unfrozen-water saturation curve was evaluated by comparing the simulation results for a single freeze-pipe freezing example with an analytical solution.

1. Introduction

Cold regions, encompassing both permafrost and seasonally freezing areas, constitute a significant portion of Earth's surface, with over 20% of the northern hemisphere's land covered by permafrost and more than 50% experiencing seasonal freezing and thawing [1]. The temperature conditions in these areas are strongly influenced by the climate, and the potential impact of climate change, particularly the freezing and thawing of frozen ground, poses a significant risk to both community safety and economic progress [2,3]. As engineering activities in cold regions continue to rise and artificial ground freezing methods become more prevalent in urban areas, research on frozen ground engineering has emerged as a primary area of interest for both scientists and geological engineering professionals. Thus, fundamental studies in frozen ground engineering and geocryology have addressed various engineering issues and explored the historical development of frozen ground engineering, along with new applications in construction engineering [4,5].

Nevertheless, achieving successful frozen ground engineering requires a thorough comprehension of frozen soil and the creation of a reliable numerical model that can anticipate ground responses during freezing. Consequently, it becomes paramount to comprehend the thermal-hydro-mechanical behavior of frozen ground under various soil conditions. The thermal–hydraulic–mechanical properties of frozen soil are influenced by the soil type, particle size and shape, and unfrozen water. Among these factors, the unfrozen-water saturation of frozen soil influences its strength, deformation, and thermal behavior [6]. Unfrozen-water saturation refers to the unfrozen moisture remaining in soil even when the soil is frozen [7,8], which is induced by adsorption forces and curvature at particle surfaces [9–12]. Unfrozen water decreases strength by enabling flexible bonding between soil particles. In certain cases, when the soil freezes, the water within its pores may migrate towards subzero regions and crystallize into ice lenses, causing severe frost-heave damage [11,13–17]. Furthermore, unfrozen water influences thermal, hydraulic, and electrical characteristics as well as mechanical behavior of soil [18–23]. Therefore, a thorough examination and understanding of the unfrozen-water characteristics of target soil are essential for a reliable assessment of the thermal–hydraulic–mechanical behavior of frozen soil.

The measurement of unfrozen water content includes various methods utilizing sensors and precision equipment, each with its own set of advantages and drawbacks. Among these, Nuclear Magnetic Resonance (NMR) emerges as the most precise technique for measurement [11,24–29]. However, its drawback lies in the high cost of equipment setup. Another approach, water potential method is advantageous for

* Corresponding author.
E-mail address: gyuhyungo@kumoh.ac.kr (G.-H. Go).

https://doi.org/10.1016/j.icheatmasstransfer.2024.107418

Available online 22 March 2024

estimating the amount of unfrozen moisture in permafrost [30–33]. This method measures the pore water potential of the sample by stepwise reducing the water content and subsequent thermodynamic calculations. It has the advantage of automatically monitoring the measured moisture potential and enabling quick measurement [34]. Another approach, Frequency Domain Reflectometry (FDR), offers continuous measurement of floating water content during freeze-thaw processes at a relatively low cost. Nevertheless, it faces limitations in accuracy, as it struggles to provide consistent values depending on pore water salt content and soil type [35,36]. Presently, many studies are employing Time Domain Reflectometry (TDR) sensors to measure the unfrozen water content of soil [37,38]. The TDR method gauges the travel time of electromagnetic waves from the probe, estimating the medium's relative permittivity and deriving the volume function ratio through a relational equation. With a reported measurement error within 0.5% when compared to the NMR method, TDR is regarded as a cost-effective alternative with excellent measurement performance [39].

Many empirical models have been proposed based on test data regarding the relationship between unfrozen-water saturation (or content) and subzero temperatures [20,24,40–47], representative models among these are presented in Table 1. As shown in Table 1, the models employ various output variables—some utilizing moisture content by weight (ω_u), some employing volumetric water content (θ_u), and some using unfrozen water saturation (χ_L). However, each output variable can easily be converted to each other using correlation equations among these variables.

Most of these models are simple and provide convenient predictions of the relationship between unfrozen water saturation and soil temperature. However, the curve-fitting coefficients in these models lack physical meaning, and a usage limit arises as it is challenging to estimate these coefficients in the absence of experimental data. Hence, gaining insight into the methodology for determining the coefficients would offer notable advantages.

This study proposes a simple methodology for reliably determining the curve-fitting coefficients included in the empirical model equation. First, a simple indoor freezing experiment was conducted to obtain time-temperature data. Then, a numerical analysis model was established in which the unfrozen water saturation curve was used as an input parameter. By iteratively conducting a numerical analysis to determine the unfrozen water saturation curve that most reasonably simulates the freezing process of the specimen, the optimal combination of curve-fitting coefficients for the unfrozen water saturation curve was determined. The reliability of the determined unfrozen-water saturation curve was examined by comparing the simulation results for a single freeze-pipe freezing example with an analytical solution.

Table 1
Empirical models calculating the unfrozen water retention curve.

Empirical Model	Form	Reference	Output variable
Zhou and Meschke model	$\chi_L = \left(1+\left(\frac{T_f-T}{\Delta T_{ch}}\right)\frac{1}{1-m}\right)^{-m}$	[20]	χ_L
Tice et al. model	$\chi_L = \left[1-\left(T-T_f\right)\right]^{\alpha}$	[24]	χ_L
Mckenzie exponential model	$\chi_L = \chi_r + (1-\chi_r)exp\left[-\left(\frac{T-T_f}{\gamma}\right)^2\right]$	[45]	χ_L
Michalowski et al. model	$\omega_u = \omega_r + (\omega_0-\omega_r)exp\left[\mu\left(T-T_f\right)\right]$	[42]	ω_u
Li et al. model	$\omega_u = \omega_r + (\omega_s-\omega_r)\frac{1}{1+(T/a)^m}$	[41]	ω_u
van Genuchten-Zhou model	$\theta_u = (\theta_s-\theta_r)\frac{1}{\left[1+a_v(-T)^{n_v}\right]^{m_v}} + \theta_r$	[40]	θ_u
Fredlund and Xing-Zhou model	$\theta_u = (\theta_s-\theta_r)\frac{1}{\left\{ln\left[e+\left(-T/a_f\right)^{n_v}\right]^{m_v}\right.} + \theta_r$	[40]	θ_u

2. Indoor freezing experiment

2.1. Needle probe test

This study aims to present a method for easily determining the fitting curve coefficient of empirical unfrozen water saturation model through simple freezing experiment data (time-temperature data) and reverse calculation of numerical analysis. To obtain reliable data on time-soil temperature from the simulation model, it is crucial to accurately input the thermal conductivity of the soil into the model. Thus, this study conducted a thermal conductivity measurements test under freezing condition. The used soil specimens were classified according to the Unified Soil Classification System as 'SP' and exhibited a specific gravity, uniformity coefficient, and curvature coefficient of approximately 2.66, 2.06, and 1.05, respectively. The initial dry density of the soil is 1380 kg/m^3 (i.e. porosity is 0.48), the initial moisture content is 34.83%. For the thermal conductivity test, the TR-3 probe in the TEMPOS measurement device [48], a non-steady-state method, was employed to measure the variation in effective thermal conductivity of the sandy soil during freezing. The probe sensor's operating temperature range is -50 °C to 150 °C. Herein, the non-steady-state probe method is a technique based on the infinite line-source theory and uses the principle of supplying a small, constant heat flux to a probe inserted into a specimen and analyzing the resulting temperature response [49]. The non-steady-state probe method is particularly useful for measuring the thermal conductivity of materials undergoing dynamic processes such as freezing. It provides a means of assessing how the thermal conductivity of a material varies under changing temperature conditions, such as during the freezing of sandy soil.

Eq. (1) represents the process whereby heat is transferred radially in a one-dimensional manner from a medium with a uniform initial temperature, starting from a heat source and Eq. (2) expresses the temperature at any arbitrary point [50]:

$$\frac{1}{\alpha_m}\frac{\partial T}{\partial t} = \frac{\partial^2 T}{\partial r^2} + \frac{1}{r}\frac{\partial T}{\partial r} \tag{1}$$

$$\Delta T(r,t) = \frac{q}{4\pi\lambda_m} ln\left(\frac{4\alpha_m t}{cr^2}\right), c = e^{r} = 1.78 \tag{2}$$

where T is the temperature, t is the time, q is the supplied heat per unit length, and α_m is the thermal diffusivity of the material. When plotting the temperature increase of the heat line against the natural logarithm of time, Eq. (3) exhibited a linear form, and the slope of the derived line and the average heat supply rate were used to measure the effective thermal conductivity of each specimen.

$$\lambda_{eff} = \frac{q}{4\pi}\frac{lnt_2 - lnt_1}{T_2 - T_1} \tag{3}$$

To check the precision of the thermal conductivity measurement sensor (TR-3 probe) before the experiment, we measured the thermal conductivity of a reference sample (silicon epoxy) at room temperature (Table 2). The thermal conductivity of each reference sample was measured repeatedly 5 times and the average value was calculated. Consequently, the measured values were confirmed to be consistent with literature values within the ±1% error range. Afterwards, this

Table 2
Comparison results of thermal conductivity measurement for the reference material.

Reference Material	Thermal conductivity [W/(m·K)]		Error(%)
silicon epoxy	1.042	1.036	0.58%

study was able to derive the thermal conductivity of the soil during the freezing process, and confirmed that the observed data fell within the range of measured values from previous research conducted on similar soil samples [51].

2.2. Freezing chamber system

The freezing chamber used in this study had dimensions of 500 mm (W) × 500 mm (D) × 600 mm (H) and was capable of cooling the internal air temperature of the chamber to a minimum of −90 °C. The sample fixation device installed within the chamber was designed to prevent detachment of the probe sensor caused by expansion due to pore-water phase changes during freezing and to constrain the volumetric expansion of samples (Fig. 1). The sample mold used was made of austenitic stainless steel (SUS316) and had a radius and height of 70 mm and 130 mm, respectively, to accommodate the sample composition. The TR-3 probe requires a minimum of 15 mm of distance parallel to the sensor in all directions to avoid measurement errors (i.e., the sensor's radius of influence is 15 mm). Therefore, the sample size used in this study far exceeds the sensor's radius of influence. A mold cap was fastened using eight bolts to provide additional resistance to the expansion deformation of the sample. Furthermore, to efficiently cool the internal temperature of the sample to below −20 °C, the chamber's internal temperature was set, and freezing tests were performed. The reader of the METER TEMPOS probe was extended to outside the chamber to enable real-time monitoring of the temperature and thermal conductivity inside the sample during freezing.

3. Numerical analysis

3.1. Governing equation

In this study, a numerical model was developed to simulate the soil freezing process. The formula for analyzing freezing soil was based on thermodynamic theory [52,53], and an approximate solution was derived for the formula using the commercial COMSOL Multiphysics software [54]. The target soil specimen was considered a three-phase structure consisting of soil particles, water, and ice. Assuming a local temperature equilibrium state, the temperature variation in the soil due to freezing was simulated using the following energy conservation equation [19,55]:

$$C_A\frac{\partial T}{\partial t}+\nabla\left(-\lambda_{eff}\nabla T\right)=0 \tag{4}$$

$$C_A=\rho C-L\frac{\partial\theta_i}{\partial T}\rho_i \tag{5}$$

where C_A is the apparent volumetric heat capacity (J/(m^3·K)), which includes a term representing the energy release due to pore-water phase changes during freezing; T is the soil temperature (K); ρ_i is the density of ice (kg/m^3); and L is the latent heat of fusion of pore water per unit mass (3.33 × 10^5 J/kg). The volumetric heat capacity (ρC) is defined as the sum of the volumetric heat capacities of the three phases multiplied by their volumetric fractions (J/(m^3·K)), and effective thermal conductivity (λ_{eff}) is defined as a function of the volumetric composition of the three phases (W/(m·K)) [19].

$$\rho C=\sum_j \rho_j C_j\theta_j, j=s,w,i \tag{6}$$

$$\lambda_{eff}=\prod_j \lambda_j^{\theta_j}, with\sum_j\theta_j=1, j=s,w,i \tag{7}$$

where θ is the volumetric fraction, and the subscripts s, w, and i represent the soil particles, pore water, and ice, respectively. The volumetric fraction of θ can be expressed as function of χ_L and porosity n.

$$\theta_s=1-n,\ \theta_w=\chi_L n,\ \theta_i=n(1-\chi_L) \tag{8}$$

where χ_L is the unfrozen-water saturation. In the numerical analysis simulating artificial ground freezing processes, the unfrozen-water saturation curve of frozen soil was used as a critical input parameter.

$$\chi_L=\left(1+\left(\frac{T_f-T}{\Delta T_{ch}}\right)^{\frac{1}{1-m}}\right)^{-m} \tag{9}$$

The unfrozen-water saturation curve model, as proposed by Zhou and Meschke [20], was employed in this study. This empirical model offers the advantages of determining the curve slope and residual saturation level by combining two curve-fitting coefficients (m and ΔT_{ch}) (see Fig. 2). Here, T_f is the freezing point of the soil (K). In this study, the freezing point of sandy soil was considered as 0 °C.

3.2. Freeze test simulation

In this study, a mathematical model was used to simulate the freezing test process of frozen sandy soil. The COMSOL PDE module was employed to apply the aforementioned governing equation and boundary conditions. In addition, the following assumptions were made to model the freezing behavior of soil.

1. The material properties are considered to be isotropic.
2. The soil is a fully saturated medium, and is considered to have a three-phase structure consisting of soil particles, water, and ice.
3. Three-phase soil materials satisfy the local thermal equilibrium.

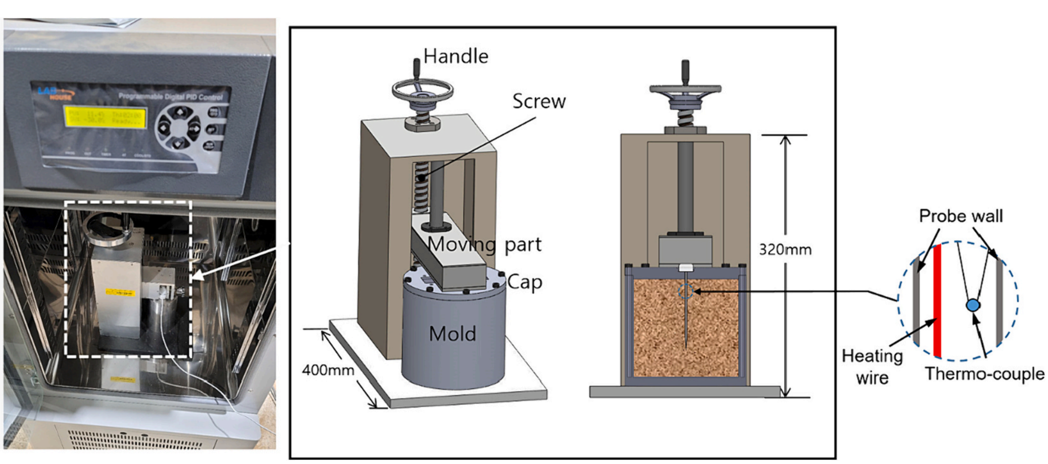

Fig. 1. Testing setup for measuring effective thermal conductivity during freezing.

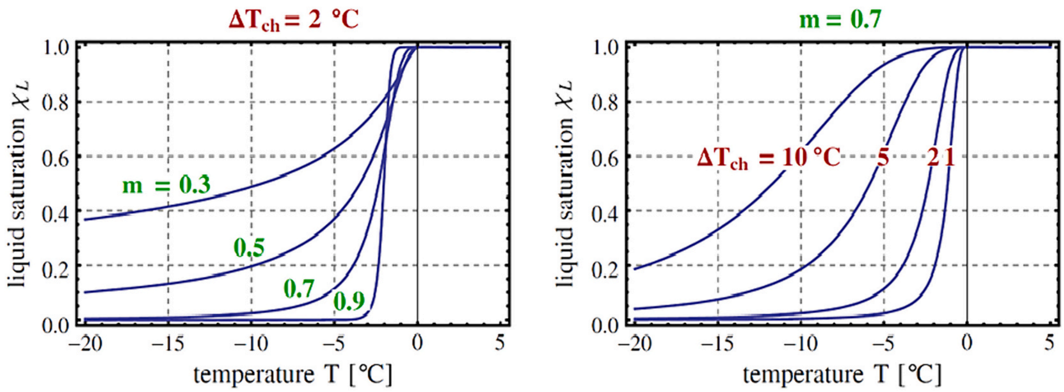

Fig. 2. Liquid-saturation curve during freezing: influence of m and ΔT_{ch} [20].

4. The effect of soil volume expansion due to pore water freezing was ignored.

To optimize the analysis efficiency, a two-dimensional axisymmetric (2D axial symmetric) model was used. As shown in Fig. 3, the analysis domain included only the specimen and mold regions. This was because the convective boundary conditions described by Eq. (10) was applied to the outermost part of the mold.

$$q|_{ext} = h(T_{ext} - T_{\mathrm{mold}}) \tag{10}$$

where T_{mold} is the temperature at the mold boundary obtained from the calculations, and T_{ext} is the air temperature inside the freezing chamber measured during the test (Fig. 4). h represents the convective heat transfer coefficient. According to the literature [56], the approximate range of convective heat transfer coefficient that can be considered when natural convection occurs in the air (gas) medium is known to be 5–25 W/(m^2·K). In this study, the median value of the presented range was applied as the convective heat transfer coefficient.

A total of 4394 square element meshes were used in the analysis, with a total analysis time of 185 min. The material properties used in the simulation are listed in Table 3.

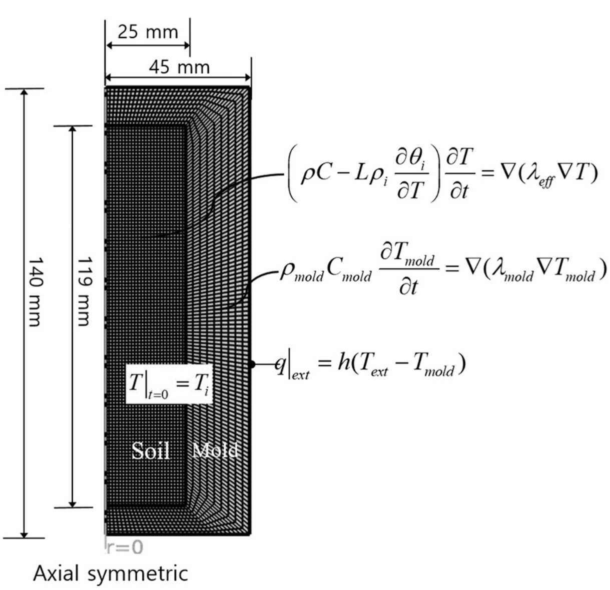

Fig. 3. Model domain, governing equation, and initial and boundary conditions.

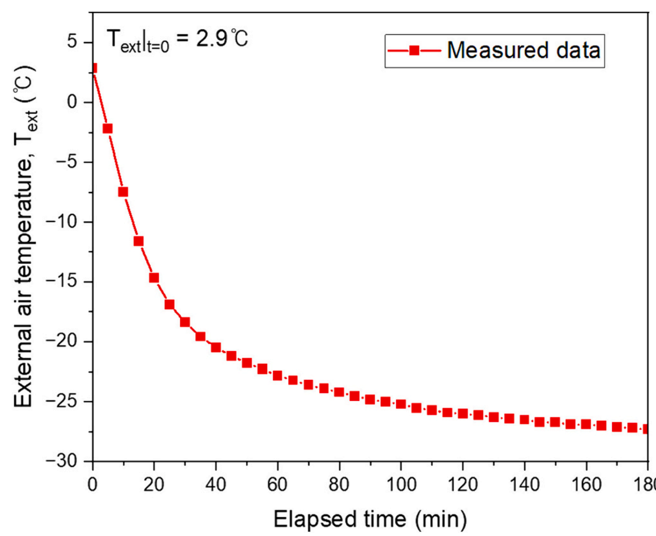

Fig. 4. Air temperature measured inside freezing chamber.

Table 3
Material properties used in simulation model.

Parameter	Symbol	Value	Unit
Porosity	n	0.48	–
Density of water	ρ_w	1000	kg/m^3
Density of ice	ρ_i	917	kg/m^3
Density of solid particle	ρ_s	2660	kg/m^3
Density of mold	ρ_{mold}	2700	kg/m^3
Heat capacity of water	C_w	4200	J/(kg·K)
Heat capacity of ice	C_i	2100	J/(kg·K)
Heat capacity of solid particle	C_s	826	J/(kg·K)
Heat capacity of mold	C_{mold}	900	J/(kg·K)
Latent heat of fusion	L	3.33E05	J/kg
Thermal conductivity of water	λ_w	0.58	W/(m·K)
Thermal conductivity of ice	λ_i	2.22	W/(m·K)
Thermal conductivity of solid particle	λ_s*	5.07	W/(m·K)
Thermal conductivity of mold	λ_{mold}	238	W/(m·K)
Convective heat transfer coefficient	h	15	W/(m^2·K)

* Data was referred to [57].

4. Analytical solution for determining the freezing-temperature distribution

Cai et al. [58] proposed an analytical solution to determine the freezing-temperature distribution in a single freeze pipe. The ground temperature distribution was divided into frozen and unfrozen zones along the freezing front (Fig. 5). The temperature distributions for each

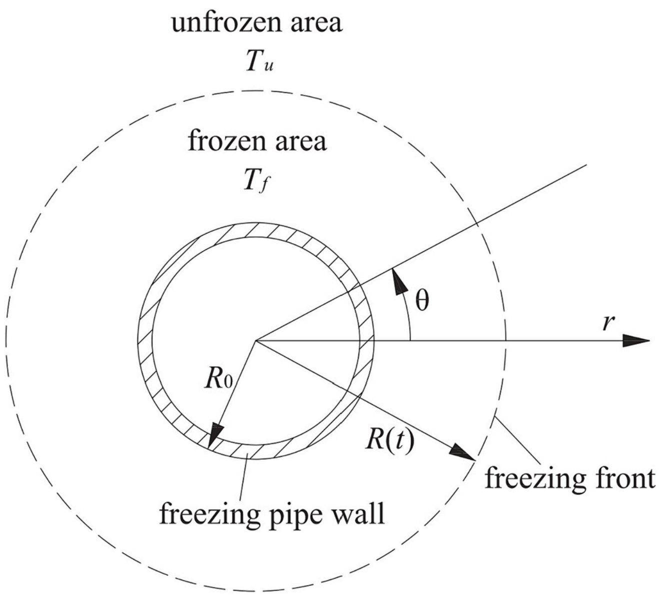

Fig. 5. Schematic of single-pipe freezing [58].

zone were calculated separately, and the analytical solutions are as follows [58]:

$$T_f = T_c + (T_d - T_c)\frac{E_i\left(\frac{R_0^2}{4\alpha_f t}\right) - E_i\left(\frac{r^2}{4\alpha_f t}\right)}{E_i\left(\frac{R_0^2}{4\alpha_f t}\right) - E_i\left(\frac{R(t)^2}{4\alpha_f t}\right)}, \quad (R_0 \le r \le R(t)) \tag{11}$$

$$T_u = T_0 + (T_d - T_0)\frac{E_i\left(\frac{r^2}{4\alpha_u t}\right)}{E_i\left(\frac{R(t)^2}{4\alpha_u t}\right)}, (R(t) \le r < \infty) \tag{12}$$

$$E_i(x) = \int_x^{\infty} \frac{e^{-\eta}}{\eta} d\eta \tag{13}$$

where T_f is the temperature of the soil in the frozen area, T_u is the temperature of the soil in the unfrozen area, and both are functions of time t and radial coordinate r. T_d is the soil temperature at the freezing front, T_0 is the initial temperature of the soil, T_c is the freezing-pipe wall temperature, R_0 is the outer radius of the freezing pipe, and $R(t)$ is the radius of the freezing front. α_f and α_u are the thermal diffusivities of frozen and unfrozen soil, respectively, and $E_i(x)$ is the exponential integral function. When considering a single-pipe freezing scenario and assuming that the thermal properties of frozen and unfrozen soil are known under a constant freeze-pipe wall temperature, the radius of the freezing front can be determined using Eqs. (14) and (15) [58].

$$\frac{k_f(T_d - T_c)e^{-\frac{\beta^2}{4\alpha_f}}}{E_i\left(\frac{R_0^2}{4\alpha_f t}\right) - E_i\left(\frac{\beta^2}{4\alpha_f}\right)} + \frac{k_u(T_d - T_0)e^{-\frac{\beta^2}{4\alpha_u}}}{E_i\left(\frac{\beta^2}{4\alpha_u}\right)} = \frac{\beta^2}{4}L \tag{14}$$

$$R(t) = \beta\sqrt{t} \tag{15}$$

where k_f and k_u the thermal conductivities of frozen soil and unfrozen soil, respectively. β is an undetermined constant, which can be obtained from Eq. (14).

5. Results and discussions

5.1. Simulation on the determination of unfrozen-water saturation curve

Fig. 6 shows the temperature variations within the specimen mold during freezing, obtained from the constructed 2D axisymmetric simulation model. Overall, the temperature deviation between the mold and specimen was relatively small (within 0.5 °C). However, during the phase change of the pore water in the soil specimen, the temperature deviation between the mold and specimen was comparatively large (Fig. 6(c)). This was attributed to the energy released from the phase change, which prevented a significant decrease in the temperature of the specimen.

A more distinct illustration of these observations is presented in Fig. 7, which shows the temperature variations in the specimen over time. After freezing, the temperature of the specimen initially decreased until it approached the freezing point of the pore water. At this point, soil freezing is delayed because of the energy released from the phase change. Subsequently, when the phase change was complete, the soil temperature began to decrease again. Such freezing behavior is determined based on the unfrozen-water saturation characteristics of the specimen. In this study, a numerical analysis model and freezing experiment data (elapsed time – temperature data) were employed to determine a combination of two curve-fitting coefficients for the empirical model proposed by Zhou and Meschke [20], aiming to establish the unfrozen water saturation curve of sand. The iterative numerical analysis identified the curve-fitting coefficient combination that best aligned with the time-temperature relationship obtained in the experiment. The simulation result using $\Delta T_{ch} = 0.5$ °C and $m = 0.7$ best fitted the experimental results (Fig. 7), and the shape of the unfrozen-water saturation curve, to which the determined coefficients were applied, is depicted in Fig. 8.

Fig. 9 shows the variation in the thermal conductivity of the sandy soil specimen during freezing. The thermal conductivity of ice is generally significantly higher than that of water (Table 2) which results in an increased effective thermal conductivity when the specimen freezes. The effective thermal conductivity of the frozen specimen increased by approximately 1.6 to 1.7 times compared to that of the unfrozen state (Fig. 9). During the pore-water phase change, there were severe fluctuations in the measured data, which can be attributed to the challenges that the small amount of heat applied by the probe sensor for the thermal conductivity measurement is unable to generate subtle temperature changes in the specimen due to interference from pore-water phase transitions [59]. Meanwhile, accurately predicting the variation in effective thermal conductivity during the phase change section is contingent on the precise calculation of the unfrozen water saturation curve (see Eqs. (7) and (8)). Once the unfrozen water saturation curve is determined, the change in thermal conductivity can also be predicted using the numerical simulation model. The numerically calculated thermal conductivities in both the frozen and unfrozen states closely matched the measured data. The RMSE between the measured data and predicted data was confirmed to be 0.255. Additionally, while obtaining reliable data within the phase change section is difficult in experiments, numerical analysis enables the observation of a continuous change in effective thermal conductivity in the subzero temperature section.

5.2. Validation of determined unfrozen-water saturation curve

The analytical solution, developed based on physics, predicts the soil freezing process and temperature distribution but employs a methodology significantly different from the one commonly used in numerical analysis. Notably, the analytical solution does not require an unfrozen water curve, a necessity in numerical simulations. Thus, this study validated the reliability of the determined unfrozen water curve by comparing numerical analysis results with the analytical solution

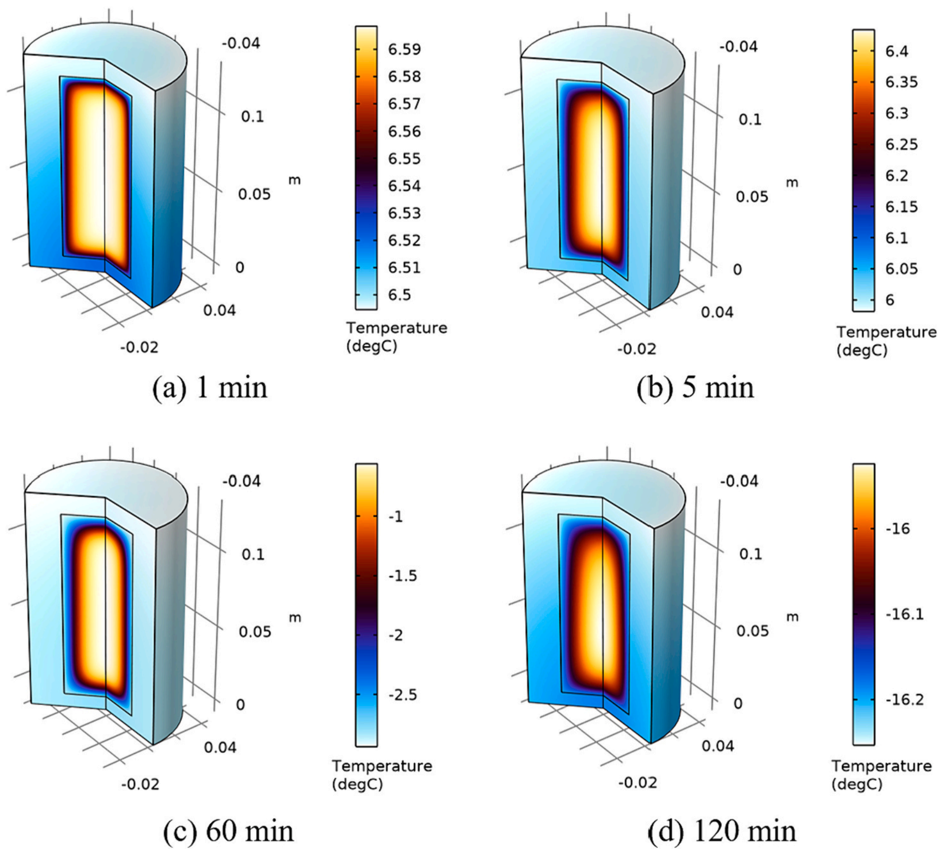

Fig. 6. Simulation results of temperature inside mold during freezing.

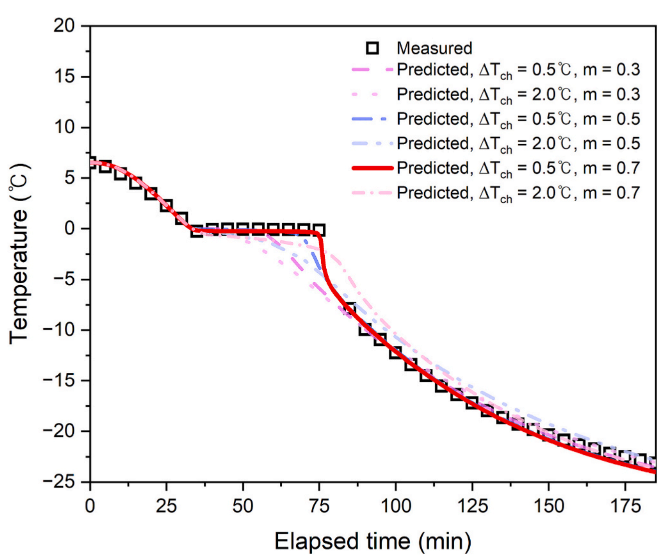

Fig. 7. Temperature change of soil specimen over time (measured data and predicted data).

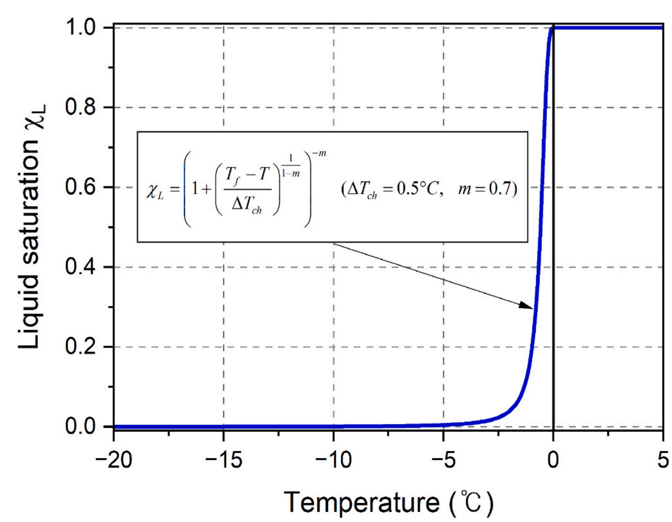

Fig. 8. Determined liquid-saturation curve for sandy soil.

proposed by Cai et al. [58]. The comparison was conducted under identical conditions (i.e., thermal properties of the soil, initial temperature conditions, and freezing boundary conditions). We examined the soil temperature distribution and radius variation of the freezing front in a benchmark problem, focusing on the freezing of a single pipe. As depicted in Fig. 10, the simulation results were consistent with the analytical solutions, demonstrating a remarkable similarity in terms of the ground temperature distribution and radius variation of the freezing front. For some cases, the numerical analysis tends to slightly overpredict the radius of the ice pillar as time elapses. This discrepancy may arise from the thermal properties of water, ice, and particles assumed in the numerical analysis. However, the magnitude of this error is deemed acceptable, considering the scale of the radius. Therefore, the unfrozen-water saturation curve obtained in this study is highly reliable and can serve as an input parameter for various analyses related to the freezing behavior of similar sandy soil.

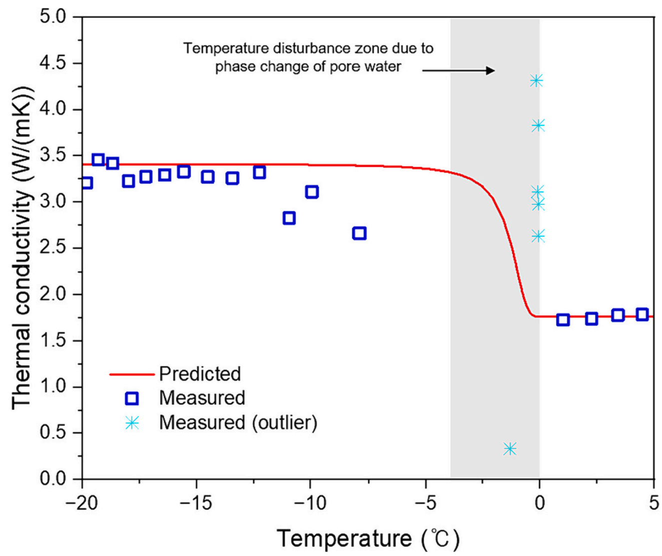

Fig. 9. Thermal conductivity variation according to temperature change.

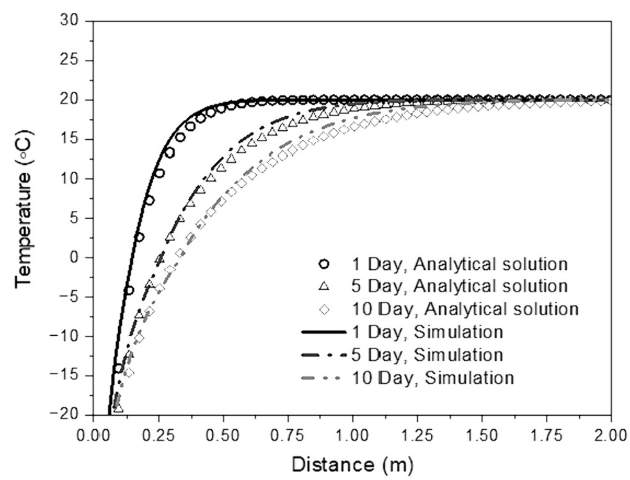

(a) Distribution of soil temperature field with radial distance

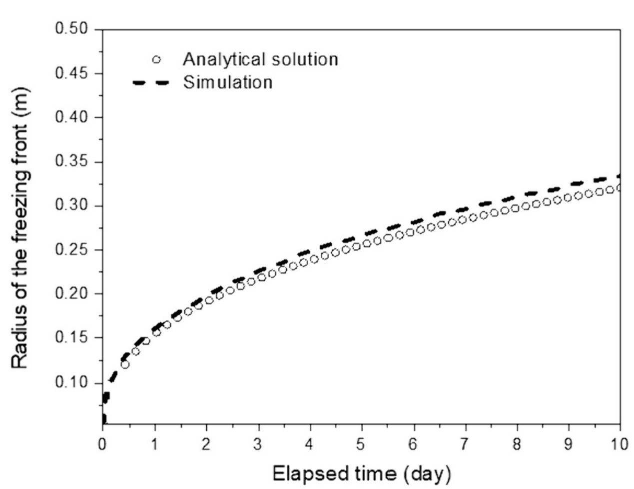

(b) Variation in the radius of freezing front with time

Fig. 10. Comparison results between simulation and analytical solution of Cai et al. [58].

6. Conclusions

The unfrozen-water saturation curve of ground material is a critical input parameter in numerical analysis for simulating the soil freezing process. This study differentiates itself from existing research by presenting a method for easily determining the fitting curve coefficient of empirical unfrozen water saturation model through simple freezing experiment data (time-temperature data) and iterative calculation of numerical analysis. An appropriate curve for the unfrozen-water saturation curve of sandy soil specimens was obtained by conducting iterative numerical analyses based on indoor experimental data. The reliability of the determined unfrozen-water saturation curve was validated by comparing the simulation results of a single freeze-pipe benchmark example with analytical solutions. The main conclusions drawn from the results are as follow:

1. During the initial stages of freezing, the temperature of soil specimens gradually decreases until it reaches the freezing point of pore water. At this point, soil freezing is delayed owing to the energy release from the phase change, and then the temperature decreases again. Such freezing behavior is highly dependent on the characteristics of the unfrozen water in the soil specimen.
2. To determine the unfrozen-water saturation curve of sandy soil specimens, iterative numerical analyses were performed based on indoor experimental data, using the empirical model proposed by Zhou and Meschke [20]. The simulation results matched the test results most accurately when a specific combination of fitting coefficients ($\Delta T_{ch} = 0.5\,^{\circ}\mathrm{C}$, $m = 0.7$) was applied to define the unfrozen-water saturation curve.
3. The effective thermal conductivity of the soil specimen in both the frozen and unfrozen states, as determined using numerical analysis, closely resembled the measured data. Additionally, the numerical analysis was able to capture continuous changes in thermal conductivity during the entire freezing process, unaffected by the phase-change region.
4. To examine the reliability of the unfrozen-water saturation curve applied in the analysis model, a simulation of a single freeze-pipe freezing benchmark was conducted under the same conditions, and the simulation results obtained using the unfrozen-water saturation curve closely matched the analytical solution. Thus, it was confirmed that the unfrozen-water saturation curve obtained in this study is highly reliable and can be considered as a valuable input parameter for future investigations concerning the freezing behavior of sandy soil.
5. Since the soil material and conditions covered in this study were limited, there are constraints in using the calculated curve-fitting coefficients universally for all soil types. Nevertheless, the methodology presented in this study is applicable regardless of the type of soil sample and the soil's condition. It is judged that an accurate unfrozen water saturation curve could also be obtained for other soils with different conditions if the methodology is applied adequately.

CRediT authorship contribution statement

Seok Yoon: Writing – review & editing, Writing – original draft, Methodology, Investigation, Formal analysis. **Gyu-Hyun Go:** Writing – review & editing, Writing – original draft, Visualization, Validation, Supervision, Software, Investigation, Funding acquisition, Conceptualization.

Declaration of competing interest

The authors declare that they have no known competing financial interests or personal relationships that could have appeared to influence the work reported in this paper.

Data availability

The data that has been used is confidential.

Acknowledgements

This work was supported by the National Research Foundation of Korea(NRF) grant funded by the Korea government(MSIT) (No. 2022R1C1C1006507).

References

[1] Y. Zhang, Thermal-Hydro-Mechanical Model for Freezing and Thawing of Soils, Doctoral dissertation, 2014.
[2] D.A. Streletskiy, N.I. Shiklomanov, F.E. Nelson, Permafrost, infrastructure and climate change: a gis-based landscape approach to geotechnical modeling, Arct. Antarct. Alp. Res. 44 (3) (2012) 368–380.
[3] P.J. Williams, M.W. Smith, The Frozen Earth. Fundamentals of Geocryology. Studies in Polar Research Series, Xvi + 306 Pp, Cambridge University Press, Cambridge, New York, Port Chester, Melbourne, Sydney, 1989.
[4] O.B. Andersland, B. Ladanyi, An Introduction to Frozen Ground Engineering, Chapman & Hall, New York, N.Y, 1994.
[5] E.D. Yershov, General Geocryology, Cambridge university press, 2004.
[6] W. Xusheng, Z. Jishuai, P. Wansheng, Z. Fengxi, L. Jianguo, Y. Zhongrui, W. Da, A theoretical model on unfrozen water content in soils and verification, J. Hydrol. 622 (2023) 129675.
[7] C. Wang, Y. Lai, M. Zhang, Estimating soil freezing characteristic curve based on pore-size distribution, Appl. Therm. Eng. 124 (2017) 1049–1060.
[8] B. Kralj, G.N. Pande, A stochastic model for the permeability characteristics of saturated cemented porous media undergoing freezing, Transp. Porous Media 22 (1996) 345–357.
[9] D.R. Uhlmann, K.A. Jackson, Frost heave in soils, Phys. Snow Ice 1 (2) (1966) 1361–1373.
[10] E.G. Hivon, D.C. Sego, Strength of frozen saline soils, Can. Geotech. J. 32 (2) (1995) 336–354.
[11] K. Watanabe, M. Mizoguchi, Amount of unfrozen water in frozen porous media saturated with solution, Cold Reg. Sci. Technol. 34 (2) (2002) 103–110.
[12] Y.C. Kim, J.H. Bae, W.K. Song, An experimental study on the unfrozen water contents and ultrasonic wave velocity in frozen soil, J. Kor. Soci. Civil Eng. 39 (6) (2002) 801–809.
[13] K. Horiguchi, R.D. Miller, Experimental studies with frozen soil in an ice sandwich permeameter, Cold Reg. Sci. Technol. 3 (1980) 177–183.
[14] T. Ishizaki, Experimental study on unfrozen water migration in porous materials during freezing, J. Nat. Disaster Sci. 17 (1995) 65–74.
[15] T. Ohrai, Experimental Studies on the Effects of Ice and Unfrozen Water on the Compressive Strength of Frozen Soil, Ph.D. dissertation,, Hokkaido University, Sapporo, Japan, 1986.
[16] E.C. Shin, J.J. Park, An experimental study on frost heaving pressure characteristics of frozen soils, J. Kor. Geotech. Soc. 19 (2003) 65–74.
[17] S.Y. Kim, W.T. Hong, S.S. Hong, Y. Back, J.S. Lee, Unfrozen water content and unconfined compressive strength of frozen soils according to degree of saturations and silt fractions, J. Kor. Geotech. Soc. 32 (12) (2016) 59–67.
[18] T.P. Burt, P.J. Williams, Hydraulic conductivity in frozen soils, Earth Surf. Proc. 1 (1976) 349–360.
[19] R.L. Michalowski, M. Zhu, Frost heave modelling using porosity rate function, Int. J. Numer. Anal. Methods Geomech. 30 (8) (2006) 703–722.
[20] M.M. Zhou, G. Meschke, A three-phase thermo-hydro-mechanical finite element model for freezing soils, Int. J. Numer. Anal. Methods Geomech. 37 (18) (2013) 3173–3193.
[21] L. Tang, K. Wang, L. Jin, G. Yang, H. Jia, A. Taoum, A resistivity model for testing unfrozen water content of frozen soil, Cold Reg. Sci. Technol. 153 (2018) 55–63.
[22] H.R. Thomas, P. Cleall, Y.C. Li, C. Harris, M. Kern-Luetschg, Modelling of cryogenic processes in permafrost and seasonally frozen soils, Geotechnique 59 (3) (2009) 173–184.
[23] Z. Lai, X. Zhao, R. Tang, J. Yang, Electrical conductivity-based estimation of unfrozen water content in saturated saline frozen sand, Adv. Civil Eng. 2021 (2021) 1–13.
[24] A.R. Tice, D.M. Anderson, A. Banin, The prediction of unfrozen water contents in frozen soils from liquid limit determinations, in: CRREL, US Army Corps of Engineers, 1976.
[25] T. Ishizaki, M. Maruyama, Y. Furukawa, J.G. Dash, Premelting of ice in porous silica glass, J. Cryst. Growth 162 (1996) 455–460.
[26] Y. Chen, Z. Zhou, J. Wang, Y. Zhao, Z. Dou, Quantification and division of unfrozen water content during the freezing process and the influence of soil properties by low-field nuclear magnetic resonance, J. Hydrol. 602 (2021) 126719.
[27] A.M. Kruse, M.M. Darrow, S. Akagawa, Improvements in measuring unfrozen water in frozen soils using the pulsed nuclear magnetic resonance method, J. Cold Reg. Eng. 32 (1) (2018) 04017016.
[28] Y. Tao, P. Yang, L. Li, X. Si, Y. Jin, Characterizing unfrozen water content of saline silty clay during freezing and thawing based on superposition of freezing point reduction, Cold Reg. Sci. Technol. 213 (2023) 103933.
[29] Y. Zou, H. Jiang, E. Wang, X. Liu, S. Du, Variation and prediction of unfrozen water content in different soils at extremely low temperature conditions, J. Hydrol. 624 (2023) 129900.
[30] V.A. Istomin, E.M. Chuvilin, B.A. Bukhanov, Fast estimation of unfrozen water content in frozen soils, Earth's Cryosphere XXI (2017) 134–139.
[31] V.A. Istomin, E.M. Chuvilin, B.A. Bukhanov, T. Uchida, Pore water content in equilibrium with ice or gas hydrate in sediments, Cold Reg. Sci. Technol. 137 (2017) 60–67.
[32] V.A. Istomin, E.M. Chuvilin, N.A. Makhonina, B.A. Bukhanov, A method for calculating the unfrozen water curve from moisture potential, in: In Proceedings of the International Conference Cryogenic Resources of the Polar and Mountainous Regions: State of the Art and Prospects of Permafrost Engineering, Tyumen, Russia, 21–24 April 2008, pp. 398–401.
[33] E.M. Chuvilin, B.A. Bukhanov, A.Z. Mukhametdinova, E.S. Grechishcheva, N. S. Sokolova, A.G. Alekseev, V.A. Istomin, Freezing point and unfrozen water contents of permafrost soils: estimation by the water potential method, Cold Reg. Sci. Technol. 196 (2022) 103488.
[34] E.M. Chuvilin, N.S. Sokolova, B.A. Bukhanov, Changes in unfrozen water contents in warming permafrost soils, Geosciences 12 (6) (2022) 253.
[35] K. Yoshikawa, P.P. Overduin, J.W. Harden, Moisture content measurements of moss (Sphagnum spp.) using commercial sensors, Permafr. Periglac. Process. 15 (4) (2004) 309–318.
[36] Z. Li, J. Chen, M. Sugimoto, Pulsed NMR measurements of unfrozen water content in partially frozen soil, J. Cold Reg. Eng. 34 (3) (2020) 04020013.
[37] E.J.A. Spaans, J.M. Baker, Examining the use of TDR for measuring liquid water content in frozen soils, Water Resour. Res. 31 (1995) 2917–2925.
[38] Z. Liu, X. Yu, Physically based equation for phase composition curve of frozen soils, Transp. Res. Rec. 2349 (2349) (2013) 93–99.
[39] M.W. Smith, A.R. Tice, Measurement of the unfrozen water con-tent of soils, in: Comparison of NMR and TDR Methods. CRREL-88-18, Cold Regions Res. Eng. Lab, Hanover, NH, 1988.
[40] J. Zhou, Experimental Study on Characteristics of Unfrozen Water in Clay Mineral and its Effect on Sand Thawing Characteristics, China University of Mining and Technology, Xuzhou, 2020.
[41] B. Li, L. Huang, X. Lv, Y. Ren, Variation features of unfrozen water content of water-saturated coal under low freezing temperature, Sci. Rep. 11 (1) (2021) 15398.
[42] R.L. Michalowski, A constitutive model of saturated soils for frost heave simulations, Cold Reg. Sci. Technol. 22 (1) (1993) 47–63.
[43] T. Osterkamp, V. Romanovsky, Freezing of the active layer on the coastal plain of the Alaskan Arctic, Permafr. Periglac. Process. 8 (1) (1997) 23–44.
[44] J. Teng, Y. Zhong, S. Zhang, D. Sheng, A mathematic model for the soil freezing characteristic curve: the roles of adsorption and capillarity, Cold Reg. Sci. Technol. 181 (2021) 103178.
[45] J.M. McKenzie, C.I. Voss, D.I. Siegel, Groundwater flow with energy transport and water–ice phase change: numerical simulations, benchmarks, and application to freezing in peat bogs, Adv. Water Resour. 30 (4) (2007) 966–983.
[46] S. Westermann, J. Boike, M. Langer, T. Schuler, B. Etzelmüller, Modeling the impact of wintertime rain events on the thermal regime of permafrost, Cryosphere 5 (4) (2011) 945–959.
[47] D.J. Nicolsky, V.E. Romanovsky, S.K. Panda, S.S. Marchenko, R.R. Muskett, Applicability of the ecosystem type approach to model permafrost dynamics across the Alaska north slope, Case Rep. Med. 122 (1) (2017) 50–75.
[48] METER group, Tempos User Manual, 2018.
[49] A.S. Mickley, The thermal conductivity of moist soil, Trans. Am. Inst. Electr. Eng. 70 (2) (1951) 789–1797.
[50] H.S. Carslow, J.C. Jaeger, Conduction of heat in solids, 2nd ed., Oxford University Press.
[51] J.F. Wright, F.M. Nixon, S.R. Dallimore, J. Henninges, M.M. Cote, Thermal conductivity of sediments within the gas-hydrate-bearing interval at the JAPEX/JNOC/GSC et al. Mallik 5L-38 gas hydrate production research well, in: Scientific Results from the Mallik 2002 Gas Hydrate Production Research Well Program, Mackenzie Delta, Northwest Territories, Canada (pp. CD-ROM). Geological survey of Canada, 2005.
[52] O. Coussy, Mechanics and Physics of Porous Solids, John Wiley and Sons, 2010.
[53] O. Coussy, P. Monteiro, Unsaturated poroelasticity for crystallization in pores, Comput. Geotech. 34 (4) (2007) 279–290.
[54] Comsol, Introduction to Comsol Multiphysics, Comsol, Inc, USA, 2023.
[55] O. Coussy, Poromechanics, John Wiley & Sons, Chichester, UK, 2004.
[56] S. Kakac (Ed.), Boilers, Evaporators, and Condensers, Wiley, New York, NY, 1991.
[57] T. Tokoro, T. Ishikawa, S. Shirai, T. Nakamura, Estimation methods for thermal conductivity of sandy soil with electrical characteristics, Soils Found. 56 (5) (2016) 927–936.
[58] H. Cai, L. Xu, Y. Yang, L. Li, Analytical solution and numerical simulation of the liquid nitrogen freezing-temperature field of a single pipe, AIP Adv. 8 (5) (2018) 055119.
[59] E. Penner, Thermal conductivity of frozen soils, CaJES 7 (3) (1970) 982–987.